SSRG International Journal of Electrical and Electronics Engineering
ISSN: 2348-8379/ https://doi.org/10.14445/23488379/IJEEE-V12I1P101

Volume 12 Issue 1, 1-8, January 2025

Original Article

Multivariate DoA Estimation of Electromagnetic Waves Arriving Spherical Antenna Array under Mutual Coupling Effects Using Higher-Order Pseudo Intensity Vector Technique

Oluwole John Famoriji[1], Thokozani Shongwe[2]

[1,2]*Department of Electrical and Electronic Engineering Technology, University of Johannesburg, P.O. Box 524, Auckland Park, Johannesburg 2006, South Africa.*

[1]*Corresponding Author : famoriji@mail.ustc.edu.cn*

Received: 01 November 2024 Revised: 03 December 2024 Accepted: 02 January 2025 Published: 25 January 2025

Abstract *- Spherical Antenna Array (SAA) can receive Electromagnetic (EM) waves with equal signal strength, regardless of polarization, Direction-of-Arrival (DoA), or angle of arrival. However, estimating DoA in a multi-source environment with a low Signal-to-Noise Ratio (SNR) remains a significant research challenge that requires technical attention. This paper introduces a novel feature-the Higher-Order Pseudo-Intensity Vector (HoPIV), derived from data obtained with an SAA. Utilizing the unique properties of the reactive intensity vector derived from HoPIV, a method is proposed for identifying time-frequency points dominated by the direct path. Consequently, a DoA estimation method is introduced, leveraging the high spatial resolution of HoPIV to enhance DoA estimation performance with a high degree of accuracy. Numerical simulations, which account for mutual coupling effects, demonstrate how the developed technique outperforms state-of-the-art methods, even at low SNR. In addition, the practical deplorability of the HoPIV-based method against baseline methods is investigated using experimental data (incorporating factors such as mutual coupling, multipath fading effects, and hardware imperfections) in electromagnetics vis-à-vis an SAA, which, in the end, the ground truth to test and evaluate any method. The results show that the proposed HoPIV-based method is preferred over the state-of-the-art method.*

Keywords *- Spherical antenna array, EM wave, DoA estimation, HoPIV, Low SNR, Mutual coupling, Multi-source.*

1. Introduction

Direction-of-Arrival (DoA) estimation has become a significant topic in Electromagnetic (EM) science, garnering attention in both industry and academia. It is widely applicable in vehicular engineering, sonar, radar, military surveillance, and wireless communication systems [1-6]. Understanding the DoA of an incoming EM wave received by an antenna is crucial for accurately localizing the sources of these signals. This knowledge enhances adaptive beamforming, allowing the system to focus on the desired direction of the EM wave while minimizing unwanted interferences [4, 5]. Consequently, the antenna can deliver maximum signal strength to users and nullify interference, improving the performance of wireless and base stations. Therefore, DoA estimation is a key focus in antenna array signal processing.

A Spherical Antenna Array (SAA) is a crucial configuration to obtain an antenna array with isotropic features. SAA is widely used in satellite and spacecraft engineering. Its electronic beam scanning capability is a quality choice whenever a hemispherical scan and almost uniform distributed gain is required [6, 7]. SAA (as shown in Figure 1) has another merit in its 3D symmetric nature, and spatial signal analysis benefits so much from it. The size and geometry of the Spherical Antenna Array (SAA) determine its directivity and the extent of beam scanning required in both azimuth and elevation [8, 9]. Consequently, accurately estimating the Direction-of-Arrival (DoA) using an SAA while accounting for mutual coupling effects continues to be challenging.

In literature, various DoA estimation techniques are proposed in the spherical harmonic domain [10, 11]. Subspace methods have been developed in the Spherical Harmonic (SH) domain [12]. The Estimation of Signal Parameter through Rotational Invariance Technique (ESPRIT) in SH domain, with the acronym ESPRIT-SH, has been proposed using a tangent function based on the SH recursive relationship. On the other hand, ESPRIT-SH becomes ill-conditioned when the tangent function approaches infinity around the spherical surface. The two-stage ESPRIT-SH method uses two successive Spherical Harmonics (SH) recurrences to estimate elevation and azimuth separately. A decoupled two-stage technique, which combines ESPRIT-SH followed by root MUSIC in SH, has also been proposed [13]. A DoA vector ESPRIT-SH approach has been used to derive directional variables from three distinct SH recurrence relations, with each variable corresponding to different components of the limit vector, ultimately pointing to the DoA [14, 15]. Li et al. [16] developed MUSIC-SH, though it requires significant computational resources due to the need for a 2D angle search [17]. Furthermore, Kumar et al. [18] introduced root MUSIC-SH, which avoids peak searching but only estimates azimuth through polynomial rooting.

(a)

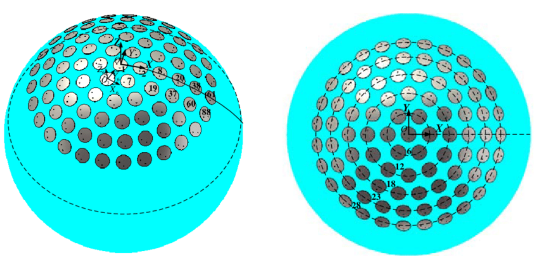

(b)

Fig. 1 Typical spherical antenna array (a) SAA with 64 elements for a conformal demonstration [8], and (b) geometry of SAA with 88 elements [9].

Lately, techniques using signal intensity vectors emerged as favourable methods for estimating DoA. Remarkably, for SAAs, two major techniques have been proposed, i.e., Pseudo Intensity Vectors (PIV) and Subspace PIV (SPIV) [19, 20]. The SPIV computes the covariance matrix in a similar way to the DPD (Direct Path Dominant) test approach and employs the first eigenvector to formulate SPIV that takes the first-order signal field information to estimate DoA [21, 22]. Although both PIV and SPIV show capability, it is important to note that the performance of PIV becomes worse when the angular separation between signal sources becomes small. This shortcoming results from low-order information obtained by PIV that may not give enough estimation of DoA with high resolution in such cases. By extension, this paper presents a method that uses the Higher-Order Pseudo-Intensity Vector (HoPIV) as a significant characteristic for detecting the DPD and DoA estimation. At first, the HoPIV formula is derived, showing its ability to detect high-order spatial information in the EM field. Secondly, it is demonstrated how the reactive part of the HoPIV becomes zero when DPD points are correlated with a source. It is worth noting that the HoPIV bring about higher-order spatial information that can be used to estimate DoA with appreciable accuracy.

2. System Model

Considering the SAA with a radius r comprising L omnidirectional radiators, SAA's origin is similar to the 3D polar coordinate system. The positions of the antenna are represented as $r_l \triangleq (r, \theta_l, \phi_l)$, r, θ_l, ϕ_l are radial distance, polar angle, and azimuth table, respectively, for the *l-th* antenna having $l = 1,2,\dots,L$, assuming the presence of $Q(Q \geq 1)$ EM sources in the signal field, which are located at the far field. The pressure of the signal at *l-th* antenna resulting from the Q plane waves could be formulated by SH decomposition as [22].

$$p_l(k, r, \theta_l, \phi_l) = \sum_{n=0}^{N} \sum_{m=-n}^{n} \sum_{q=1}^{Q} b_n(kr) \left[Y_n^m(\theta_q, \phi_q)\right]^* \cdot Y_n^m(\theta_l, \phi_l) s_q(k) + n_l(k), \quad (1)$$

Where, $b_n(kr)$ denotes the strength of mode obtained from rigid and open spherical arrays, $[\cdot]^*$ is the conjugation operation, k is the wave number, (θ_q, ϕ_q) are the angle of elevation and the azimuth of q-th source, respectively. $s_q(k)$ represents the amplitude of the q-th source, $n_l(k)$ is the additive noise. $Y_n^m(\cdot)$ represents the SH of order n and degree m, and it is expressed as [23].

$$Y_n^m(\theta, \phi) = \sqrt{\frac{2n+1}{4\pi} \frac{(n-m)!}{(n+m)!}} P_n^m(\cos\theta) e^{im\phi} \quad (2)$$

Where $P_n^m(\cdot)$ is the associated Legendre function, $i = \sqrt{-1}$ denoting the imaginary unit. This paper presents the analysis and estimation performed in the SH domain. Let us assume an ideal SH transform, implying the EM wave pressures received by SAA in Equation. (1) are correctly presented as a function of SH components. The SH decomposition coefficient is defined as,

$$a_{nm}(k) = \sum_{q=1}^{Q} \left[Y_n^m(\theta_q, \phi_q)\right]^* s_q(k) + \bar{n}_{nm}(k), \quad (3)$$

Where $n = 0, \dots, N$, $m = -n, \dots, n$, and $\bar{n}_{nm}(k)$ represents the noise SH decomposition components. In all, only $(N+1)^2$ SH decomposition coefficients exist. The matrix form of Equation (3) is expressed as [24].

$$a(k) = Y^H(\boldsymbol{\varphi}) s(k) + \bar{n}(k) \quad (4)$$

The matrix $Y^H(\varphi)$ is the steering matrix corresponding to the direction of the source, i.e.

$$Y^H(\varphi) = \left[y^*(\varphi_1) \ldots y^*(\varphi_1) \ldots y^*(\varphi_Q)\right], \tag{5}$$

$\varphi = [\varphi_1 \ldots \varphi_q \ldots \varphi_Q]$ is the corresponding 2D plane wave DoAs, with $\varphi_q \triangleq [\theta_q, \phi_q]$, and

$$y(\varphi_q) = \left[Y_0^0(\varphi_q) \ldots Y_n^m(\varphi_q) \ldots Y_N^N(\varphi_q)\right]^T$$

$$a(k) = [a_{00}(k) \ldots a_{nm}(k) \ldots a_{NN}(k)]^T,$$

$$s(k) = \left[s_1(k) \ldots s_q(k) \ldots s_Q(k)\right]^T,$$

$$\bar{n}(k) = [\bar{n}_{00}(k) \ldots \bar{n}_{nm}(k) \ldots \bar{n}_{NN}(k)]^T.$$

The complex steering matrix is transformed into a real steering matrix to give room for DPD detection. The matrix of transformation is given as,

$$\Theta = \frac{1}{\sqrt{2}}\begin{bmatrix} iI_n & 0_n & (-1)^n iJ_n \\ 0_n^T & \sqrt{2} & 0_n^T \\ G_n & 0_n^T & J_n G_n \end{bmatrix}, \tag{6}$$

I_n represents the $n \times n$ identity matrix, G_n is the matrix that is not diagonal, having ones in non-diagonal locations, zeros elsewhere, 0_n is a $n \times 1$ column vector, and J_n is given as,

$$J_n = \begin{bmatrix} & & -1 \\ & \ldots & \\ (-1)^n & & \end{bmatrix}. \tag{7}$$

If Equation (4) is multiplied by Θ, it yields.

$$\hat{a}(k) = \hat{Y}^T(\varphi)s(k) + \hat{n}(k), \tag{8}$$

$\hat{a}(k)$ and $\hat{n}(k)$ represent the transformed signal and noise vector, respectively. $\hat{\boldsymbol{Y}}^T(\boldsymbol{\varphi})$ is the $(N+1)^2 \times Q$ real steering matrix, and

$$\hat{a}(k) = [\hat{a}_{00}(k) \ldots \hat{a}_{nm}(k) \ldots \hat{a}_{NN}(k)]^T,$$

$$\hat{n}(k) = [\hat{n}_{00}(k) \ldots \hat{n}_{nm}(k) \ldots \hat{n}_{NN}(k)]^T,$$

$$\hat{\boldsymbol{Y}}^T(\boldsymbol{\varphi}) = [\hat{y}(\varphi_1) \ldots \hat{\boldsymbol{y}}(\varphi_q) \ldots \hat{y}(\varphi_Q)],$$

$$\hat{y}(\varphi_q) = \left[\hat{Y}_0^0(\varphi_q) \ldots \hat{Y}_n^m(\varphi_q) \ldots \hat{Y}_N^N(\varphi_Q)\right]^T,$$

$\hat{Y}_n^m(\cdot)$ represents the real SH [11] having order n and degree m and expressed as,

$$\hat{Y}_n^m(\theta, \phi) = \begin{cases} \sqrt{\frac{2n+1}{2\pi}\frac{(n-|m|)!}{(n+|m|)!}} P_n^m(cos\theta) \sin(|m|\phi), & m < 0 \\ \sqrt{\frac{2n+1}{4\pi}} P_n^m(cos\theta), & m = 0 \\ \sqrt{\frac{2n+1}{2\pi}\frac{(n-m)!}{(n+m)!}} P_n^m(cos\theta) \cos(m\phi) & m > 0 \end{cases} \tag{9}$$

Since the signal processing is analyzed in the short-time Fourier transform (STFT) domain, $\hat{a}_{nm}$ is then given similarly as,

$$\hat{a}_{nm}(\zeta, \varsigma) = \sum_{q=1}^{Q} \hat{Y}_n^m(\theta_q, \phi_q)\, s_q(\zeta, \varsigma) + \hat{n}_{nm}(\zeta, \varsigma) \tag{10}$$

Where ζ, ς represents the time frame and frequency bin index, correspondingly.

3. Developed Technique

3.1. HoPIV

Motivated by the method in [21] that employs the zero-order and first-order SH coefficient for the velocity approximation of pressure and particle, the HoPIV is defined as,

$$\Gamma(\zeta, \varsigma) \triangleq [\,\Gamma_{00}(\zeta, \varsigma)\ \ldots\ \Gamma_{nm}(\zeta, \varsigma) \ldots \Gamma_{NN}(\zeta, \varsigma)]^T \tag{11}$$

$$\Gamma_{nm}(\zeta, \varsigma) \triangleq \hat{a}_{nm}(\zeta, \varsigma)\widehat{a^*}_{00}(\zeta, \varsigma) \tag{12}$$

The real part and the imaginary part of $\Gamma_{nm}(\zeta, \varsigma)$, i.e. $\Re\{\Gamma_{nm}(\zeta, \varsigma)\}$ and $\Im\{\Gamma_{nm}(\zeta, \varsigma)\}$ are noted to be the active and the reactive components of HoPIV, respectively. Then, neglecting the noise term of Equation (10) with a multi-plane wave superposition scenario, $\hat{a}_{nm}(\zeta, \varsigma)$ and $\hat{a}_{00}(\zeta, \varsigma)$ can be modified to be,

$$\hat{a}_{nm}(\zeta, \varsigma) = \sum_{q=1}^{Q} \hat{Y}_n^m(\theta_q, \phi_q)\left|s_q(\zeta, \varsigma)\right| e^{i\angle s_q(\zeta, \varsigma)}, \tag{13}$$

$$\hat{a}_{00}(\zeta, \varsigma) = \sum_{q=1}^{Q} \hat{Y}_0^0(\theta_q, \phi_q)\left|s_q(\zeta, \varsigma)\right| e^{i\angle s_q(\zeta, \varsigma)} \tag{14}$$

$\angle$ is the angle of operation. In a simple manner, representing the $\angle s_q(\zeta, \varsigma)$ as $\alpha_q \Gamma_{nm}(\zeta, \varsigma)$, $\Gamma_{nm}(\zeta, \varsigma)$ results to,

$$\Gamma_{nm}(\zeta, \varsigma) = \left(\sum_{q=1}^{Q} \hat{Y}_n^m(\theta_q, \phi_q)\left|s_q(\zeta, \varsigma)\right| e^{i\alpha q}\right)\left(\sum_{q=1}^{Q} \frac{1}{\sqrt{4\pi}}\left|s_q(\zeta, \varsigma)\right| e^{i\alpha q}\right)^* \tag{15}$$

By mathematics, Equation (15) becomes

$$\Gamma_{nm}(\zeta, \varsigma) = \frac{1}{\sqrt{4\pi}}\Big[\sum_{q=1}^{Q} \hat{Y}_n^m(\theta_q, \phi_q)\left|s_q(\zeta, \varsigma)\right|^2 + \sum_{q=1}^{Q-1}\sum_{q'=q+1}^{Q}\left|s_q(\zeta, \varsigma)\right|\Big] \cdot \Big[\left|s_{q'}(\zeta, \varsigma)\right| \cos(\alpha_q - \alpha_{q'})\left(\hat{Y}_n^m(\theta_q, \phi_q) + \hat{Y}_n^m(\theta_{q'}, \phi_{q'})\right)\Big] + \frac{i}{\sqrt{4\pi}}[(\sum_{q=1}^{Q-1}\sum_{q'=q+1}^{Q}\left|s_q(\zeta, \varsigma)\right|\left|s_{q'}(\zeta, \varsigma)\right| \sin(\alpha_q - \alpha_{q'}) \cdot \left(\hat{Y}_n^m(\theta_q, \phi_q) - \hat{Y}_n^m(\theta_{q'}, \phi_{q'})\right)]. \tag{16}$$

In the multi-plane wave superposition case, the imaginary part of Equation (16) is not zero. This implies that the reactive vector component is available. Nevertheless, in the case of a single source, for example, just the q-th plane wave is available; Equation (16) is then transformed to,

$$\Gamma^{q}{}_{nm}(\zeta,\varsigma) = \frac{1}{\sqrt{4\pi}}\hat{Y}_n^m(\theta_q,\phi_q)\left|s_q(\zeta,\varsigma)\right|^2. \tag{17}$$

The disappearance of the imaginary part means the reactive intensity vector can be used to identify the direct path point by transforming the real-valued steering matrix. This characteristic limits the efficiency of using the real part of the steering matrix when used for direct path detection.

3.2. Detection

Applying the reactive intensity vector characteristics, the estimation of the reactive intensity norm that is relative to the active intensity gives,

$$\Gamma(\zeta,\varsigma) = \frac{1}{e^{(\|\Re\{\Gamma(\zeta,\varsigma)\}\|_2/\|\Im\{\Gamma(\zeta,\varsigma)\}\|_2}}, \tag{18}$$

The measurable DPD points satisfying the scenario is,

$$\Omega_{DPD} = \{(\zeta,\varsigma):\quad if\ \Gamma(\zeta,\varsigma) \geq \epsilon\}, \tag{19}$$

$\|\cdot\|_2$ represents the l_2 norm. It depicts that when the $\Gamma(\zeta,\varsigma)$ is bigger than a threshold pre-set, ϵ, the respective time frame bin gets detected as a DPD point. The DPD points set is denoted as Ω_{DPD}.

Illustrating the detection ability, three different plane waves coming from three sources at far field incident from $(35^0, 35^0)$, $(80^0, 35^0)$, and $(180^0, 35^0)$, respectively. White Gaussian noise is added at an SNR of 15 dB. We generated the sum of 3000 snapshots. Figure 2 shows the results obtained. For Figure 2 (a), the blue, green, and red colored dots are correspondingly the Γ value of one plane wave, superposition of two plane waves, and superposition of three plane waves.

In the case of a source case, Γ is almost unity and bigger compared to the values for two and three sources. Figure 2 (b) and Figure 2 (c) share the same trend as Figure 2 (a). Specifically, for HoPIV, Γ shows an observable disparity among different source superpositions.

3.3. DoA

Inspired by the connection between the direction of HoPIV and the plane wave incident direction presented by the SH functions in Equation (13), the HoPIV is employed, i.e., $\Gamma(\zeta,\varsigma)$, of DPD points in the estimation of sources' DoA. A space of direction that spans between 0 to 180 degrees by elevation and 0 to 360 degrees by azimuth is first defined.

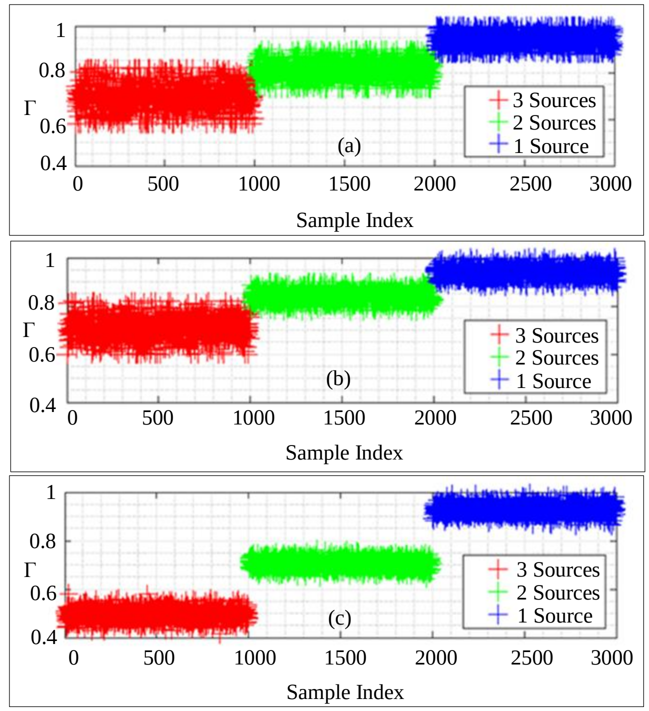

Fig. 2 The Γ for the superposition of single, two, and three plane waves under various HoPIV orders. (a) $N = 1$, (b) $N = 2$, and (c) $N = 3$.

The space is discretized into $N_\theta \times N_\phi$ number of samples, and $\Psi = [\theta, \phi]$ label is assigned to individual discrete sample pairs. The direction of propagation of plane wave in real SH function is represented by $\hat{y}(\Psi)$.

The measurement of similarity between $\Gamma(\zeta,\varsigma)$ and $\hat{y}(\Psi)$ gives the DoA of each point of DPD. The DoA estimation is accomplished by the identification of the minimum Euclidean distance between $\Gamma(\zeta,\varsigma)$ and $\hat{y}(\Psi)$ as,

$$\Psi_s = \left\{\Psi: \underset{\Psi\in\Psi}{\operatorname{argmin}}\|\Gamma(\zeta,\varsigma) - \hat{y}(\Psi)\|_2 \quad \forall(\zeta,\varsigma) \in \Omega_{DPD}\right\} \tag{20}$$

In order to enhance the degree of robustness of the estimation of DoA, the results of estimation for the DPD points detected in Ψ_s got smoothed by the developed 2D histogram smoothing technique in [19].

4. Numerical Simulation, Experiment, Results, and Discussion

Here, experimental results from both the simulation and measured experimental data are presented to illustrate the efficiency of the developed approach. The proposed technique is consequently compared against the baseline methods: SPIV, PIV [21], DPD-MUSIC [16], and DRHC [20] methods. The performance metric is the root-Mean Square Angular Error (RMSAE).

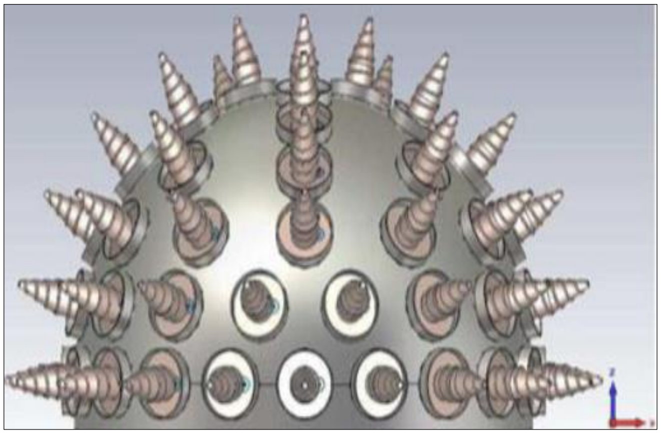

(a)

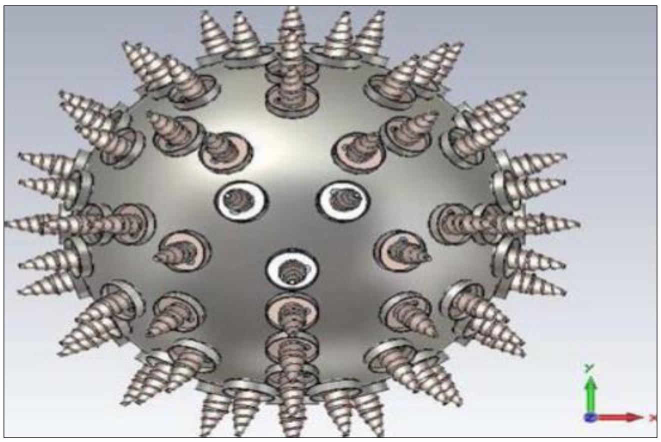

(b)

Fig. 3 The simulated SAA from CST software for verification purpose. (a) Sideward view, and (b) Aerial view.

4.1. Simulation

An SAA made up of 64-element of radius 4.2 cm that operates at 8 GHz was simulated via CST software, as described in Figure 3. Several sources were concurrently active, and the arriving EM waves were quantified by SAA. For easy analysis, an open spherical array is employed. Nonetheless, the developed approach can be directly applied to rigid arrays by incorporating the scattering factor. Data were generated using CST. The SAA's data generated in the time domain were affected by random noise in the array elements. The data were then transformed into the frequency domain using STFT.

The signals are obtained from the array via the convolution of the source signals with their respective impulse response. There is an addition of white noise to the entire channel using 20 dB SNR. 30 random positions are chosen to situate the three active sources to show how effective the developed technique is in estimating the DoAs in comparison against the baseline approaches. The sum of source signals considered is 20, with a length of about 2 sec.

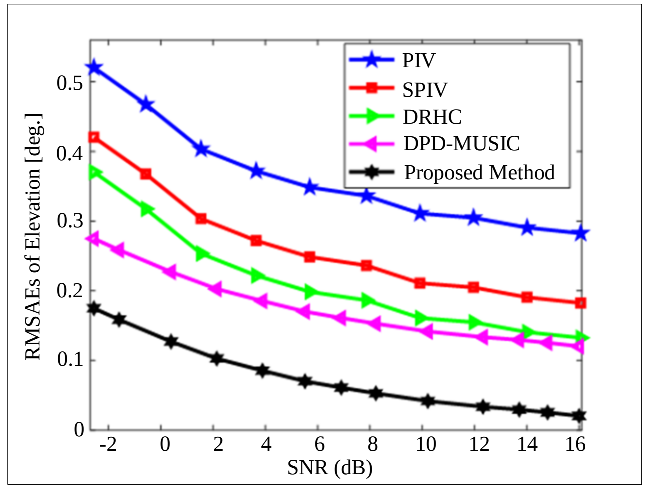

(a)

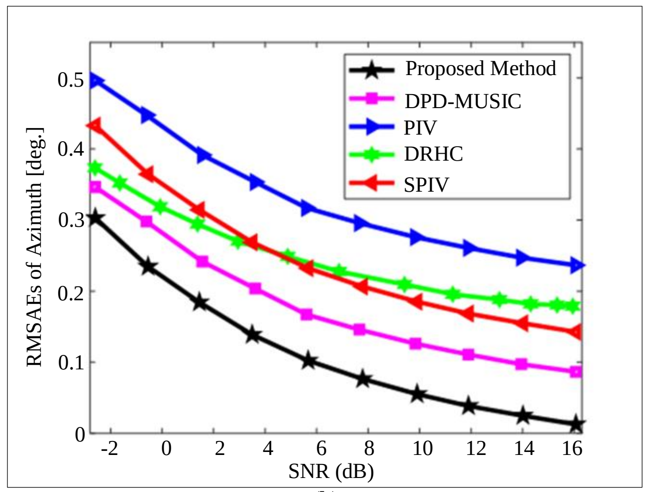

(b)

Fig. 4 The plot of RMSAE for multi-source estimation of DoA. (a) Elevation, and (b) Azimuth.

The RMSAE results obtained for each method is presented in Figure 4 (a, b). It is noted that every result shown is the average of 300 trials of signal blocks where the location of EM wave, noise, and sources are generated randomly. It can be observed that all the approaches considered or investigated exhibit performance degradation as SNR increases in Figure 4. The PIV technique that does not incorporate any DPD is affected notably by SNR and exhibits the most significant errors in estimation. Contrary to the PIV, the SPIV technique employing the first eigenvector of the time-frequency smooth covariance matrix for the first-order PIV shows marginal performance compared to the PIV. Nonetheless, it does not match the high-order techniques like DPD-MUSIC and DRHC leveraging on the high resolution spatial information to get a better estimation of DoA. The DPD-MUSIC exhibits enhanced results due to incorporating DPD and the high-resolution subspace DoA estimation. On the other hand, it has accuracy challenges in detecting all sources, as it prioritises the intense energy sources within a zone, causing potential omission of other sources. The developed technique shows consistency in its exhibition of the least RMSAE. The results show how the integration of HoPIV characteristics appreciably enhances the techniques' efficiency, making it possible to identify DPD points, which is an enabler of high-resolution DoA estimation.

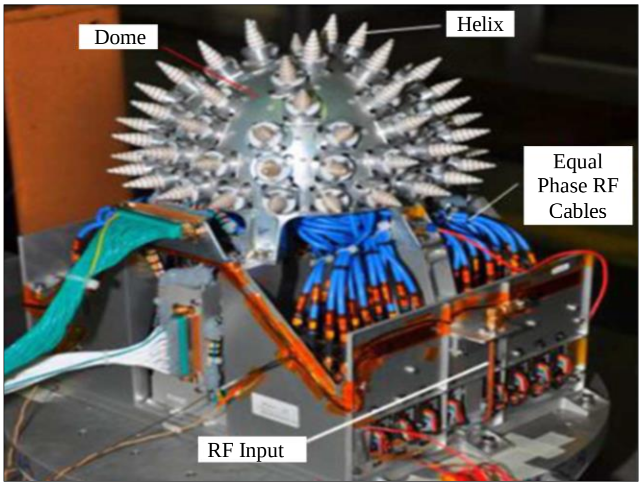

Fig. 5 The SAA in the anechoic chamber used for the experiment

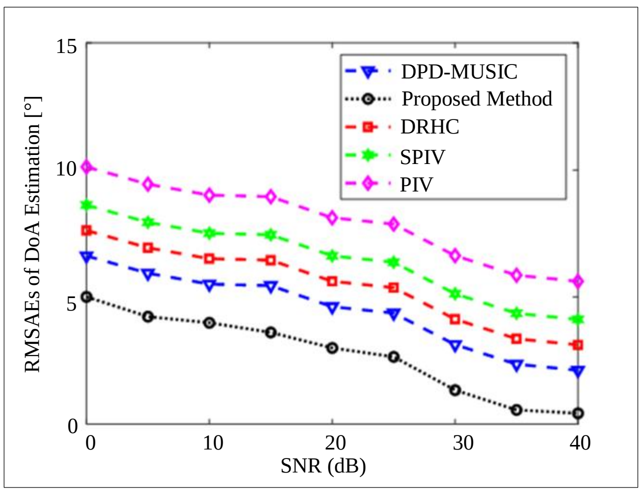

Fig. 6 The plot of RMSAE for multi-source estimation of DoA using SAA practical measured data.

4.2. Experiment

As the technology develops, current and future systems require smaller spacing between the elements. This causes severe mutual coupling, leading to unwanted antenna radiation and impedance matching. To incorporate the effects of mutual coupling, measured experimental samples-considered the ground truth to evaluate any method-were employed to test the effectiveness of all the techniques. For the measurement, the SAA is positioned at the center of the anechoic chamber with sources situated at DoAs of about 74, which were captured from a different mix of 18 elevations and azimuths. The azimuth range chosen is 5^0 to 365^0 with *a* step size 20^0. For further information on the experimental setup involving the SAA, refer to our previous work, where the original data were published.

The RMSAE of the experimental results for the DoA estimation for all methods are depicted in Figure 6. This shows that azimuth estimation generally has bigger errors, while elevation estimation exhibits more accuracy. This can be attributed to the nature of the anechoic chamber, which has no external noise. The developed HoPIV-based approach exhibits the least RMSAE, while the DRHC technique relative to SPIV shows the worst performance, which depicts a deviation from the simulation results. The deviation is because the DoA estimation deteriorates for the DRHC approach as the angle tends to the horizontal plane. Hence, the HoPIV method performs better than the state-of-the-art, even in practical situations.

4.3. Computational Cost Analysis

A complexity analysis of the proposed method is performed compared to baseline methods by measuring the elapsed run-time. All computations are done using Matlab on a computer with the following specifications: 8th Generation Intel Core i7 processor, 16 GB RAM, 64-bit operating system, and a 1TB SDR. Experimental data are used to calculate the run-time for each method.

Table 1 presents the average elapsed run time comparison across grid resolutions of [1, 2, 5] degrees for various snapshot numbers (N) and DoA search grids. The PIV method demonstrates the shortest run-time. The proposed HoPIV-based method significantly reduces computation cost (run-time) compared to SPIV, DPD-MUSIC, and DRHC. While the PIV method is less costly regarding run-time, the HoPIV-based method outperforms it regarding detection accuracy.

Table 1. Elapse run-time of the proposed HoPIV method against the baseline methods

N	PIV (s)	SPIV (s)	DPD-MUSIC (s)	DRHC (s)	HoPIV (s)
10	0.019	0.025	0.162	0.154	0.021
55	0.221	0.245	0.333	0.342	0.224
70	0.190	0.280	0.435	0.386	0.192
100	0.633	0.644	0.788	0.774	0.635

5. Conclusion and Future Direction

In conclusion, a novel approach for multi-source DoA estimation in challenging environments with low SNR has been developed using a spherical antenna array (SAA) under the influence of mutual coupling. The method leverages the spatial resolution capabilities of the higher-order pseudo-intensity vector (HoPIV) to enhance the accuracy of DoA estimation and direct path detection (DPD).

By leveraging the distinctive properties of the reactive intensity vector derived from HoPIV, this technique effectively identifies time-frequency points dominated by the direct path, enhancing DoA estimation performance. The effectiveness of this approach has been demonstrated through simulations and experiments, showing that it outperforms existing methods in terms of accuracy. These promising results suggest the potential for industrial application of the developed technique. Despite the promising results presented in this study, several concerns remain that warrant further investigation. Future work will aim to extend this research by focusing on the calibration and measurement of time delay across various applications, comparing these methods with state-of-the-art techniques in terms of computational complexity, and assessing their robustness against confounding factors that can affect practical SAA applications. Therefore, HoPIV can potentially drive significant advancements in SAA processing and related applications, including mobile communication systems, aerospace, and radar systems.

Funding Statement

The Article Processing Charge (APC) is sponsored by the University of Johannesburg, South Africa.

Acknowledgment

The authors acknowledge the contribution of Mr. T. D. Makanju during the preparation of the final edition (formatting) of the manuscript.

References

[1] Matteo Carlin et al., “Directions-of-Arrival Estimation through Bayesian Compressive Sensing Strategies,” *IEEE Transactions on Antennas and Propagation*, vol. 61, no. 7, pp. 3828-3838, 2013. [CrossRef] [Google Scholar] [Publisher Link]

[2] Mariana G. Pralon et al., “Suitability of Compact Antenna Arrays for Direction-of-Arrival Estimation,” *IEEE Transactions on Antennas and Propagation*, vol. 65, no. 12, pp. 7244-7256, 2017. [CrossRef] [Google Scholar] [Publisher Link]

[3] M.A. Preston, and J.P. Lyons, “A Switched Reluctance Motor Model with Mutual Coupling and Multi-Phase Excitation,” *IEEE Transactions on Magnetics*, vol. 27, no. 6, pp. 5423-5425, 1991. [CrossRef] [Google Scholar] [Publisher Link]

[4] V.Y. Vu et al., “Measurement of Direction-of-Arrival of Coherent Signals Using Five-Port Reflectometers and Quasi-Yagi Antennas,” *IEEE Microwave and Wireless Components Letters*, vol. 15, no. 9, pp. 558-560, 2005. [CrossRef] [Google Scholar] [Publisher Link]

[5] Wen Ding, Deliang Liang, and Hongliang Sui, “Dynamic Modeling and Performance Prediction for Dual-Channel Switched Reluctance Machine Considering Mutual Coupling,” *IEEE Transactions on Magnetics*, vol. 46, no. 9, pp. 3652-3663, 2010. [CrossRef] [Google Scholar] [Publisher Link]

[6] Chandrakanta Kumar et al., “Dual Circularly Polarized Spherical Phased-Array Antenna for Spacecraft Application,” *IEEE Transactions on Antennas and Propagation*, vol. 61, no. 2, pp. 598-605, 2013. [CrossRef] [Google Scholar] [Publisher Link]

[7] B. Pavan Kumar et al., “Active Spherical Phased Array Design for Satellite Payload Data Transmission,” *IEEE Transactions on Antennas and Propagation*, vol. 63, no. 11, pp. 4783-4791, 2015. [CrossRef] [Google Scholar] [Publisher Link]

[8] Jihong Zhang et al., “A Method to Optimize Cross-Polarizarion of Full Polarimetric Conformal Antenna Array”, *2016 Progress in Electromagnetic Research Symposium (PIERS)*, Shanghai, pp. 1990-1993, 2016. [CrossRef] [Google Scholar] [Publisher Link]

[9] Peter Knott, “Design and Experimental Results of A Spherical Antenna Array for a Conformal Array Demonstrator,” *2007 2nd International ITG Conference on Antennas*, Germany, pp. 120-123, 2007. [CrossRef] [Google Scholar] [Publisher Link]

[10] Qinghua Huang, Lin Zhang, and Yong Fang, “Two-Stage Decoupled DOA Estimation Based on Real Spherical Harmonics for Spherical Arrays,” *IEEE/ACM Transactions on Audio, Speech, and Language Processing*, vol. 25, no. 11, pp. 2045-2058, 2017. [CrossRef] [Google Scholar] [Publisher Link]

[11] Qinghua Huang, Lin Zhang, and Yong Fang, “Two-Step Spherical Harmonics ESPRIT Type Algorithms and Performance Analysis,” *IEEE/ACM Transactions on Audio, Speech, and Language Processing*, vol. 26, no. 9, pp. 1684-1697, 2018. [CrossRef] [Google Scholar] [Publisher Link]

[12] Adrian Herzog, and Emanuel A.P. Habets, “Eigenbeam-ESPRIT for DOA-Vector Estimation,” *IEEE Signal Processing Letters*, vol. 26, no. 4, pp. 572-576, 2019. [CrossRef] [Google Scholar] [Publisher Link]

[13] Heinz Teutsch, *Modal Array Signal Processing: Principles and Applications of Acoustic Wavefield Decomposition*, Lecture Notes in Control and Information Sciences, Springer, New York, USA, 2007. [Google Scholar]

[14] Heinz Teutsch, and Walter Kellermann, “Eigen-Beam Processing for Direction-of-Arrival Estimation Using Spherical Apertures,” *Proceedings of the 1st Joint Workshop Hands-Free Speech Communication Microphone Arrays (HSCMA)*, USA, 2005. [Google Scholar]

[15] Byeongho Jo, and Jung-Woo Choi, “Parametric Direction-of-Arrival Estimation with Three Recurrence Relations of Spherical Harmonics,” *Journal of the Acoustical Society of America*, vol. 145, pp. 480-488, 2019. [CrossRef] [Google Scholar] [Publisher Link]

[16] Xuan Li et al., “Spherical Harmonics MUSIC versus Conventional MUSIC,” *Applied Acoustics*, vol. 72, no. 9, pp. 646-652, 2011. [CrossRef] [Google Scholar] [Publisher Link]

[17] Lalan Kumar, Guoan Bi, and Rajesh M. Hegde, “The Spherical Harmonics Root-MUSIC,” *2016 IEEE International Conference on Acoustics, Speech and Signal Processing (ICASSP)*, Shanghai, China, pp. 3046-3050, 2016. [CrossRef] [Google Scholar] [Publisher Link]

[18] M.A. Doron, and E. Doron, "Wavefield Modeling and Array Processing. II. Algorithms," *IEEE Transactions on Signal Processing*, vol. 42, no. 10, pp. 2560-2570, 1994. [CrossRef] [Google Scholar] [Publisher Link]

[19] Alastair H. Moore, Christine Evers, and Patrick A. Naylor, "Direction of Arrival Estimation in the Spherical Harmonic Domain Using Subspace Pseudointensity Vectors," *IEEE/ACM Transactions on Audio, Speech, and Language Processing*, vol. 25, no. 1, pp. 178-192, 2017. [CrossRef] [Google Scholar] [Publisher Link]

[20] Yonggang Hu, Thushara D. Abhayapala, and Prasanga N. Samarasinghe, "Multiple Source Direction of Arrival Estimations Using Relative Sound Pressure Based MUSIC," *IEEE/ACM Transactions on Audio, Speech, and Language Processing*, vol. 29, pp. 253-264, 2021. [CrossRef] [Google Scholar] [Publisher Link]

[21] Daniel P. Jarrett, Emanuel A.P. Habets, and Patrick A. Naylor, "3D Source Localization in the Spherical Harmonic Domain Using A Pseudointensity Vector," *2010 18th European Signal Processing Conference*, Denmark, pp. 442-446, 2010. [Google Scholar] [Publisher Link]

[22] Vishnuvardhan Varanasi, Harshit Gupta, and Rajesh M. Hegde, "A Deep Learning Framework for Robust DOA Estimation Using Spherical Harmonic Decomposition," *IEEE/ACM Transactions on Audio, Speech, and Language Processing*, vol. 28, pp. 1248-1259, 2020. [CrossRef] [Google Scholar] [Publisher Link]

[23] Boaz Rafaely, *Fundamentals of Spherical Array Processing*, 2nd ed., Springer, 2019. [CrossRef] [Google Scholar] [Publisher Link]

[24] Vishnuvardhan Varanasi, and Rajesh Hegde, "Robust Online Direction of Arrival Estimation Using Low Dimensional Spherical Harmonic Features," *2017 IEEE International Conference on Acoustics, Speech and Signal Processing (ICASSP)*, USA, pp. 511-515, 2017. [CrossRef] [Google Scholar] [Publisher Link]